RAPID COMMUNICATIONS

PHYSICAL REVIEW E VOLUME 50, NUMBER 5 NOVEMBER 1994

Particle-in-cell simulations of Raman forward scattering from short-pulse high-intensity lasers

C. D. Decker,[1] W. B. Mori,[1] and T. Katsouleas[2]

[1]*Departments of Physics and Electrical Engineering, University of California at Los Angeles, Los Angeles, California 90024*

[2]*Department of Electrical Engineering, University of Southern California, Los Angeles, California 90089*

(Received 5 April 1994)

We present one- and two-dimensional particle-in-cell simulations of short-pulse ($\tau<1$ ps) high-intensity ($I\leq 10^{18}$ W/cm^2) laser propagation through an underdense plasma. The simulations model near-term experiments without the limitations of the fluid and quasistatic approximations. We find that Raman forward scattering plays a dominant role in the evolution of the pulse in distances less than a Rayleigh length. Raman forward scattering results in significant spectral cascading and energetic electron generation from wave breaking of the resulting plasma wave. Both of these effects should be useful as experimental diagnostics.

PACS number(s): 52.40.Nk, 52.35.Mw, 52.40.Db

The development of advanced accelerators [1], advanced light sources [2], and advanced fusion concepts [3] necessitates an understanding of the evolution of an intense short pulse laser propagating through plasma. In laser acceleration [1,4] and optical-field-ionized recombination x-ray laser concepts [5], laser pulses must propagate relatively stably through uniform plasmas over distances greatly exceeding the diffraction length. On the other hand, in the fast ignitor inertial fusion concept [3], intense pulses must efficiently convert their energy into MeV electrons after propagating through nonuniform underdense plasmas. Therefore, any anomalous absorption and scattering in the underdense region needs to be minimized.

As a result there has been much recent interest in studying the self-focusing [6] and beam breakup of short-pulse high-intensity lasers propagating in plasmas. In some recent studies [7–9] fluid equations were numerically integrated using the quasistatic approximation. The paraxial-ray and weakly relativistic approximations [8,9] were also sometimes used. All of these approximations are inherently limiting. Fluid models do not allow for wave breaking and energetic electron generation. The quasistatic approximation [10] assumes that the laser pulse is static during a pulse duration. Therefore, it is only valid for laser pulse lengths less than the e-folding time of the beam breakup at the back of the pulse [11]. In addition, it does not allow for low phase velocity plasma waves, such as those produced in Raman backscattering [12] (RBS) and Raman sidescattering [13] (RSS). The paraxial-ray approximation precludes direct Raman forward scattering [11], and as a consequence leads to the conclusion [8] that the amount of beam breakup and self-focusing depends only on the laser power normalized to the critical power [6] for relativistic self-focusing, $P_c=17(\omega_0^2/\omega_p^2)$ GW, the propagation distance normalized to a Rayleigh length, $L_R=(\omega_0/2c)r_0^2$, and the pulse length normalized to c/ω_p, where ω_0 is the laser frequency and r_0 is the spot size.

In this paper we present one-dimensional (1D) and 2D simulations which model near-term experiments. Although the quasistatic and paraxial-ray approximations are useful for elucidating some of the above processes, we find for the experimental parameters [14,15] of many near-term experiments that such approximations are invalid. Theory and simulations reveal that for existing pulse lengths ($\sim$500 fs) and plasma densities exceeding 2×10^{18} cm^{-3} (assuming a 1 μm laser), the quasistatic approximation is invalid. The laser pulse is found to initially break up from direct Raman forward scattering (RFS) and near-forward side scattering (RSS) in distances less than a Rayleigh length. Both of these processes are precluded when the paraxial-ray approximation is used. The most dominant experimental signatures of RFS and RSS are spectral cascading (Stokes and anti-Stokes sidebands) and the generation of multi-MeV electrons.

In a recent paper [11], we derived the spatial-temporal behavior of RFS for arbitrarily large pump strengths. The exact response for the initial evolution for the plasma wave, growing from an initially spatially uniform noise source of δn_s which remains constant at the front of the pulse, is given by

$$\delta n=\begin{cases}\delta n_s\cosh(\gamma_0\tau) & \text{for } \psi>\tau\\ \delta n_s\sum\limits_n\left(\dfrac{\psi}{\tau-\psi}\right)^n I_{2n}(2\gamma_0\sqrt{(\tau-\psi)\psi}) & \text{for } \psi<\tau\end{cases} \tag{1}$$

where I_{2n} is the modified Bessel function of the first kind, ψ is the distance from the head of the pulse normalized to c/ω_p, and τ is the time normalized to ω_p. The temporal growth rate γ_0 was calculated to all orders in a_0 and found to be

$$\gamma_0=\frac{\omega_p^2}{\sqrt{8}\,\omega_0}\frac{a_0}{\sqrt{1+a_0^2/2}}, \tag{2}$$

where $a_0=eA/mc^2$, A is the vector potential of the laser, and ω_0 is the laser frequency. We note that using the quasistatic approximation gives $\delta n=\delta n_s I_0(2\gamma_0\sqrt{\tau\psi})$ which agrees with Eq. (1) when $\tau\gg\psi$. However, for $\tau\leq\psi$ the quasistatic approximation can significantly overestimate the amount of growth. In addition, we mention that the $I_0[2\gamma_0\sqrt{(\tau-\psi)\psi}]$ part of Eq. (1) is the Green's function.

We have studied the evolution of short laser pulses in both one and two dimensions using the code ISIS. We first present results from a 1D simulation done to verify the amplitude scaling of Eq. (2). The simulations were done for symmetric ultrashort pulses which had a flat top region. The length of

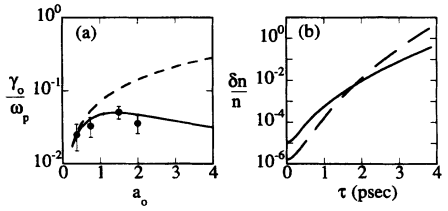

FIG. 1. (a) Temporal growth rate γ_0 versus pump strength a_0 for $\omega_0/\omega_p=5$ from simulations (circles), Eq. (2) (solid line), and the weakly relativistic four-wave growth rate (dashed line). (b) Amount of RFS growth for $a_0=0.8$, $\omega/\omega_p=10.0$, $l_0=150$ (solid line), and $l_0=75$ (dashed line).

the flat top region, L_0, was such that $\gamma_0 L_0 \ll 1$ and the rise and fall time were chosen such that the ponderomotively excited wake was small. The simulations were analyzed for $\tau \gg L_0$ because in this regime the I_0 term in Eq. (1) is dominant and the solution is simply $\delta n \simeq \delta n_s I_0(2\gamma_0\sqrt{\tau\psi})$. Therefore, we can easily obtain γ_0 by best fitting the ψ dependence from the simulation results for a given value of τ. The results are shown in Fig. 1(a) where we plot the growth rate γ_0 from simulations (circles) versus pump strength a_0 for $\omega_0/\omega_p=5$. In addition, we plot Eq. (2) (solid line) and the weakly relativistic growth rate (dashed line). We see good agreement between the simulations and Eq. (2). The error bars in Fig. 1(a) are due to the fact that the pulses do not have constant amplitude and the front of the pulse ($\psi=0$) is not well defined as a result of the finite rise time.

To predict the onset of RFS in experiments, we need to know the noise source δn_s as well as the growth rate. The ponderomotive force associated with the rise time of a short pulse can excite a large phase velocity plasma wave and for typical pulse lengths this noise source greatly exceeds the thermal noise. An expression for the amplitude of the plasma wave excited by a laser pulse with a sinusoidal profile can be obtained exactly [16]. However, for profiles used in the particle-in-cell (PIC) codes and of existing lasers, the integration must be done numerically. We find a best fit expression for the wake due to the profile used in the PIC codes to be

$$\frac{\delta n_s}{n_0} \simeq 0.9\pi \frac{a_0^2}{(k_p l_0)^q}, \tag{3}$$

where the exponent is roughly $q=2.0$ for $k_p l_0 \leq 10$ and $q=2.8$ for $k_p l_0 > 10$. We emphasize that the scaling of the wake's amplitude with l_0 depends critically upon the pulse shape and therefore, Eq. (3) should only be used as a guide. We have also verified Eq. (3) with PIC simulations and found very good agreement. By using Eq. (3) for the noise source in the spatial temporal solution of Eq. (1) the amount of RFS in an experimental situation can be estimated. For example, we consider the parameters at Lawrence Livermore National Laboratory (LLNL) [15], where a 1 μm laser with a 600 fs rise time and an intensity $I=8.9\times10^{17}$ W/cm^2 propagates through a plasma of density $n_0=10^{19}$ cm^{-3}. The normalized parameters for this case are $a_0=0.8$, $\omega/\omega_p=10.0$, and $l_0=150c/\omega_p$ and they lead to $\delta n_s/n_0=1.2\times10^{-6}$ and $\gamma_0=0.028$. In Fig. 1(b), we plot Eq. (1) as a function of τ at the position $\psi=l_0$ for this noise source and temporal growth rate. For comparison, curves for both $l_0=150$ (dashed line) and $l_0=75$ (solid line) are shown. We see that for $l_0=150$, RFS becomes significant at about 2.6 ps (0.8 mm) where $\delta n/n_0=0.1$ (This is a distance of a Rayleigh length for a 17 μm spot size.)

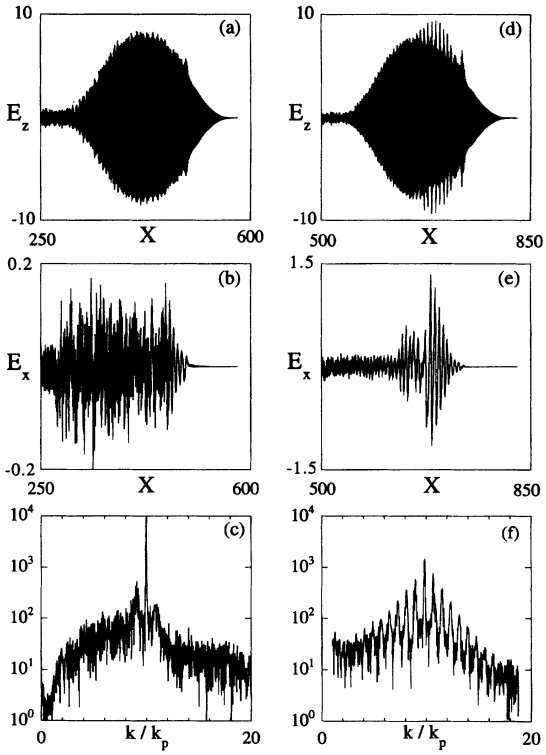

FIG. 2. Results from a 1D simulation with $a_0=0.8$, $\omega/\omega_p=10.0$, and $l_0=150c/\omega_p$. (a) Laser field $eE_z/mc\omega_p$, (b) plasma wave field $eE_x/mc\omega_p$, and (c) Fourier spectrum $E_z(k)$ at $\omega_p t=250$; (d) laser field, (e) plasma wave field, and (f) Fourier spectrum at $\omega_p t=550$. The x axis is in units of c/ω_p.

We next present results from 1D simulations to demonstrate the effect of 1D RFS for the LLNL parameters. The simulations were done using a version of ISIS in which the computational window moves with the laser pulse [17]. In Fig. 2, we plot the electric field of the laser pulse, the electric field of the resulting plasma wave, and the Fourier spectrum of the laser's electric field at $\omega_p t=250$ (1.4 ps) and $\omega_p t=500$ (2.8 ps). At $\omega_p t=250$, Raman backscattering (RBS) is dominant and RFS is beginning to occur at the head of the pulse. The pulse distortion caused by the local pump depletion due to RBS appears to provide an anomalously large noise source from which RFS grows. RBS depletes the laser energy because it grows and saturates within the same narrow region of the pulse due to its large growth rate. This can be seen in Figs. 2(a) and 2(b) where the location of the onset of RFS corresponds to the location in the laser pulse where RBS appears to cause pump depletion. This scenario was corroborated by doing an otherwise identical run in which the electron temperature was raised to suppress RBS by Landau damping. In this case RFS did not occur until $\omega_p t \sim 500$ (2.8 ps). The seeding of RFS by RBS has also been discussed by others for different simulation conditions [18].

At $\omega_p t=500$ the laser pulse has broken up and the plasma

wave has reached wave breaking amplitudes. Wave breaking generates multi-MeV electrons and is discussed later. The beam breakup occurs because of the variation in group velocity caused by density modulations of the plasma wave. This variation in group velocity leads to intensity modulations which reinforce the density modulations and for this reason RFS is sometimes referred to as a modulational instability [12]. The nonlinear state of the beam breakup leads to spectral cascading [12] as seen in Fig. 2(f). For these parameters experimentally detectable signals out to the tenth ($\omega_0+10\omega_p=2\omega_0$) sideband are observed. Spectral cascading can be viewed locally as photon acceleration [19] and deceleration. Those portions of the laser pulse which reside in regions of the plasma wave where $\nabla n<0$ ($\nabla n>0$) will be frequency upshifted (downshifted). The periodicity of this phenomena at the plasma wavelength generates the sidebands separated by the plasma frequency.

This 1D simulation illustrates the limitations of both the paraxial-ray and quasistatic approximations. The paraxial-ray approximation precludes 1D RFS, but the simulation shows that 1D RFS can lead to substantial (near 100%) beam breakup in distances on the order of a few pulse lengths. For planned experimental conditions these distances are less than a Rayleigh length. The validity of the quasistatic approximation requires that the laser does not change during a laser pulse transit time, i.e., $2l_0/c$. However, Figs. 2(a) and 2(d) taken at two times separated by a pulse transit time show substantial alterations of the pulse. Furthermore, RBS indirectly seeds RFS and it is precluded in the quasistatic approximation. We note that we have also done a simulation with mobile ions with a mass ratio of $M/m=1000$ and obtained similar results.

We next present results from a 2D simulation in x-y slab geometry to investigate the relative importance of Raman scattering (backscattering, sidescattering, and forwardscattering), relativistic self-focusing and cascade focusing [20], and the accuracy of the paraxial-ray approximation. A typical 2D simulation had the parameters $a_0=0.75$, $\omega/\omega_p=5.0$, $l_0=50$, and $r_0=9c/\omega_p$ which corresponds to $I=0.8\times10^{18}$ W/cm^2, $n=4\times10^{19}$ cm^{-3}, and $\tau_0\simeq100$ fs for a 1 μm laser. For these parameters [21] $P/P_c=1.6$ and $L_R=200c/\omega_p$. These parameters could be achieved in near-term experiments. Sample results are shown in Fig. 3. Contour plots of transverse and longitudinal electric fields are plotted for $\omega_pt=100$, $\omega_pt=150$, and $\omega_pt=250$ in Figs. 3(a) and 3(b), 3(c) and 3(d), and 3(e) and 3(f), respectively. The pulse is clearly modulated before propagating a Rayleigh length, which is when relativistic self-focusing would occur for $P/P_{cr}\simeq1$. We find that beam breakup is initially caused by 1D RFS. This is confirmed by comparing slice plots at different radial positions for the 2D runs with 1D runs for the corresponding laser amplitude. The onset for beam modulation is nearly identical. This 1D behavior is qualitatively seen at the front of the pulse at $\omega_pt=100$ where the modulation of the laser and the resulting plasma wave are somewhat planar. However, at later times, or equivalently at the back of the pulse, the beam breakup is assisted by the focusing caused by the density depression of the plasma wave. This process is related to cascade focusing [20] in beat wave excitation. However, it does not lead to coherent focusing because the density depressions lag the laser intensity peaks by $\pi/2$. The

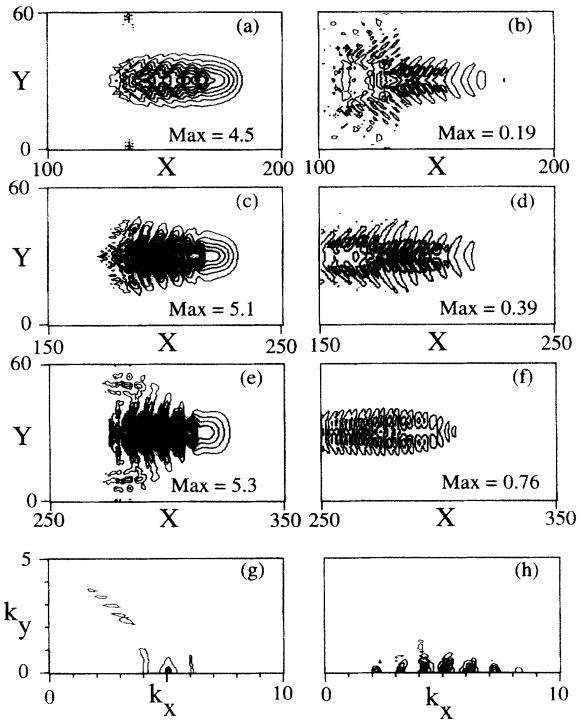

FIG. 3. Contour plots from a 2D simulation with $a_0=0.75$, $\omega/\omega_p=5.0$, and $l_0=50c/\omega_p$. (a) laser field $eE_x/mc\omega_p$ and (b) plasma wave field $eE_x/mc\omega_p$ at $\omega_pt=100$; (c) laser field and (d) plasma wave field at $\omega_pt=150$; (e) laser field and (f) plasma wave field at $\omega_pt=250$. The x and y axes are in units of c/ω_p. Fourier spectrum of laser field at (g) $\omega_pt=250$ and (h) $\omega_pt=250$. Both k_x and k_y in units of $k_p=\omega_p/c$.

phase difference arises because a harmonic oscillator oscillates $\pi/2$ out of phase with a resonant driver. The $\pi/2$ phase shift leads to the arrowhead ($\lhd$) shaped contours in Figs. 3(a) and 3(c) because the rear of the intensity modulation is focused while the forward part is not. The new intensity modulation generates plasma waves with the crescent ($<$) shaped contours [Figs. 3(b) and 3(d)]. These new density depressions further deform the laser intensity contours until the laser pulse has broken apart transversely into filaments. The resulting plasma wave also breaks apart as shown in Fig. 3(f). This entire process occurs in a distance on or less than a Rayleigh length. We note that this will occur sooner for long pulses because more spatial growth can occur [11]. In addition, we find that for longer pulses the 2D focusing in the plasma wave also leads to an earlier onset of beam breakup. The transmitted light spectrum can be a useful experimental diagnostic for RFS. We plot the Fourier spectrum of the laser's electric field at $\omega_pt=100$ and $\omega_pt=250$ in Figs. 3(g) and 3(h), respectively. At $\omega_pt=100$ the spectrum shows the laser, and the Stokes and anti-Stokes sidebands. In addition, there is a substantial amount of Raman sidescatter (RSS). RSS has only a downshifted Stokes component because the anti-Stokes cannot be simultaneously resonant. The sidescattering causes light to leave the focal region thereby reducing the local laser power. The Fourier spectrum shows all of the possible side bands at $\omega_pt=250$. The fact that most of the scattered light is confined to the focal region axis

indicates that 1D RFS is dominant. The amount of sidebands generated is similar in 1D and 2D simulations. We note that the evolution of the laser pulse can be different for small spot sizes, i.e., $r_0 \sim c/\omega_p$. In this case the laser expels the plasma electrons [22], which either eliminates or greatly reduces RFS. Simulations with small spot sizes show little Stokes and anti-Stokes signals [11].

This 2D simulation also clearly illustrates the limitations of the paraxial-ray and fluid approximations. The paraxial-ray approximation requires that $\int dy a_0^2(y)$ remain constant [9] and therefore precludes longitudinal bunching of the laser energy [11,23]. The importance of allowing longitudinal bunching for cases in which beam breakup does not occur was examined recently by Chen and Sudan [23]. It is apparent from visually examining Figs. 3(a), 3(c), and 3(e) that $\int dy a_0^2(y)$ is not constant, therefore longitudinal bunching is also important during beam breakup. The fluid approximation cannot model wave breaking which occurs when a portion of one wavefront overtakes another. Therefore, the plasma waves generated by RFS and beam breakup are less coherent than those generated in fluid codes. Additionally as in the 1D case, we find that the laser pulse evolves substantially in a pulse transit time. This is clearly seen in Figs. 3(a), 3(c), and 3(e) where the plots are taken at times separated by roughly a transit time. The above approximations will become more reasonable as the pulse length is shortened and/or the frequency ratio ω_0/ω_p increases. However, other PIC runs and fluid simulations indicate that 1D RFS is essential for the proper modeling of the initial beam breakup.

Finally, we find that invariably the plasma wave generated by RFS and beam breakup evolves to wave breaking amplitudes [Fig. 2(e)] and generates multi-MeV electrons. The p_x/mc versus x phase space is shown in Figs. 4(a) and 4(b) for the 1D and 2D simulations described earlier. The maximum energies are approximately given by $2\epsilon(\omega_0^2/\omega_p^2)mc^2$ [4] where $\epsilon = eE_x/mc\omega_p$, in both cases. Note that a significant number of accelerated electrons are generated in 2D

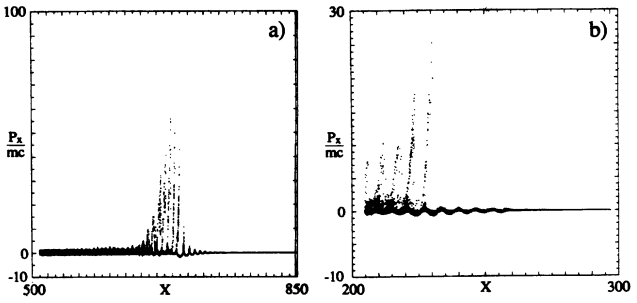

FIG. 4. Phase space plots p_x/mc versus x. (a) 1D simulation (Fig. 2); (b) 2D simulation (Fig. 3).

even though the plasma wave has the complicated structure shown in Fig. 3. Based on the simulations we estimate that the number of multi-MeV electrons generated by focusing a 5 TW 1 μm laser into a 4×10^{19} cm^{-3} plasma to be 10^9. Therefore, the detection of self-trapped electrons is another experimental diagnostic for RFS.

In summary, we have performed 1D and 2D PIC simulations of short-pulse high-intensity laser plasma interactions over long propagation distances. These simulations indicate that existing laser pulses will break up longitudinally in distances less than a Rayleigh length. Therefore, it is difficult to observe self-focusing without the earlier occurrence of RFS. We find that 1D RFS theory provides a reasonable estimate for the onset of beam breakup and that dominant experimental signatures of RFS are spectral cascading and multi-MeV electron generation.

This work was supported by DOE Grant Nos. DE-FG03-92ER40727 and DE-FG03-93ER40776 and LLNL task nos. 20 and 32. We acknowledge useful conversations with G. Shvets, C. Coverdale, and Dr. C. B. Darrow, Dr. C. McKinstrie, Dr. D. E. Hinkel, Dr. E. Esarey, Dr. P. Mora, Dr. C. Joshi, Dr. J. M. Dawson, and Dr. J. Wurtele.

[1] IEEE Trans. Plasma Sci **PS-15** (2) (1987), special issue on plasma-based high-energy accelerators, edited by T. Katsouleas, and references therein.

[2] IEEE Trans. Plasma Sci. **PS-21** (1) (1993), special issue on generation of coherent radiation using plasmas, edited by W. B. Mori, and references therein.

[3] M. Tabek, Bull. Am. Phys. Soc. **38**, 2010 (1993).

[4] T. Tajima and J. M. Dawson, Phys. Rev. Lett. **43**, 267 (1979); C. Joshi *et al.*, Nature **311**, 525 (1984).

[5] P. Amendt *et al.*, Phys. Rev. Lett. **66**, 2589 (1991); D. C. Eder *et al.*, Phys. Rev. A **45**, 6761 (1992).

[6] C. E. Max *et al.*, Phys. Rev. Lett. **33**, 209 (1974); P. Sprangle *et al.*, in Ref. [1], p. 1222.

[7] P. Sprangle *et al.*, Phys. Rev. Lett. **69**, 2200 (1992); J. Krall *et al.*, Phys. Rev. E **48**, 2157 (1993); E. Esarey *et al.*, Phys. Rev. Lett. **72**, 2887 (1994).

[8] T. M. Antonsen, Jr. and P. Mora, Phys. Rev. Lett. **69**, 2204 (1992); Phys. Fluids B **5**, 1091 (1992).

[9] N. E. Andreev *et al.*, JETP Lett. **571**, 2200 (1992).

[10] P. Sprangle *et al.*, Phys. Rev. Lett. **64**, 2011 (1990).

[11] W. B. Mori *et al.*, Phys. Rev. Lett. **72**, 1482 (1994); C. Decker *et al.* (unpublished).

[12] D. W. Forslund *et al.*, Phys. Fluids **8**, 1002 (1975); **8**, 10 117 (1975); J. F. Drake *et al.*, *ibid.* **4**, 1002 (1974); K. Estrabrook and W. L. Kruer, *ibid.* **26**, 1892 (1983).

[13] D. W. Forslund *et al.*, Phys. Rev. Lett. **54**, 558 (1985).

[14] A. B. Borisov *et al.*, Phys. Rev. Lett. **68**, 2309 (1992).

[15] C. B. Darrow *et al.*, Phys. Rev. Lett. **69**, 442 (1992).

[16] P. Sprangle *et al.*, Appl. Phys. Lett. **53**, 2146 (1988).

[17] C. D. Decker and W. B. Mori, Phys. Rev. Lett. **72**, 490 (1994).

[18] S. V. Bulanov *et al.*, Phys. Fluids B **4**, 1935 (1992).

[19] S. C. Wilks *et al.*, Phys. Rev. Lett. **69**, 1383 (1992).

[20] P. Gibbon and T. Bell, Phys. Rev. Lett. **61**, 1599 (1988).

[21] $P/P_{cr} = r_0^2 a_0^2/32$ in 3D and $r_0^2 a_0^2/20$ in 2D.

[22] G. Z. Sun *et al.*, Phys. Fluids **30**, 526 (1987); W. B. Mori *et al.*, Phys. Rev. Lett. **60**, 1298 (1988).

[23] X. L. Chen and R. N. Sudan, Phys. Fluids B **5**, 1336 (1992).

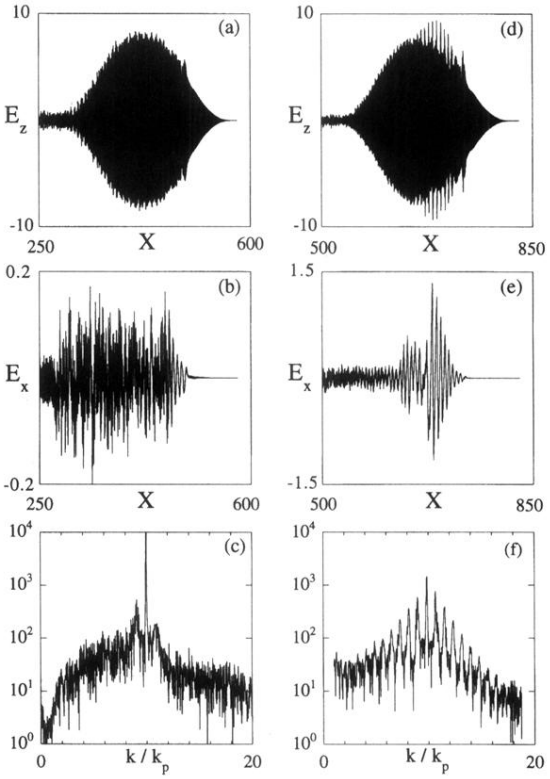

FIG. 2. Results from a 1D simulation with $a_0 = 0.8$, $\omega/\omega_p = 10.0$, and $l_0 = 150c/\omega_p$. (a) Laser field $eE_z/mc\omega_p$, (b) plasma wave field $eE_x/mc\omega_p$, and (c) Fourier spectrum $E_z(k)$ at $\omega_p t = 250$; (d) laser field, (e) plasma wave field, and (f) Fourier spectrum at $\omega_p t = 550$. The x axis is in units of c/ω_p.

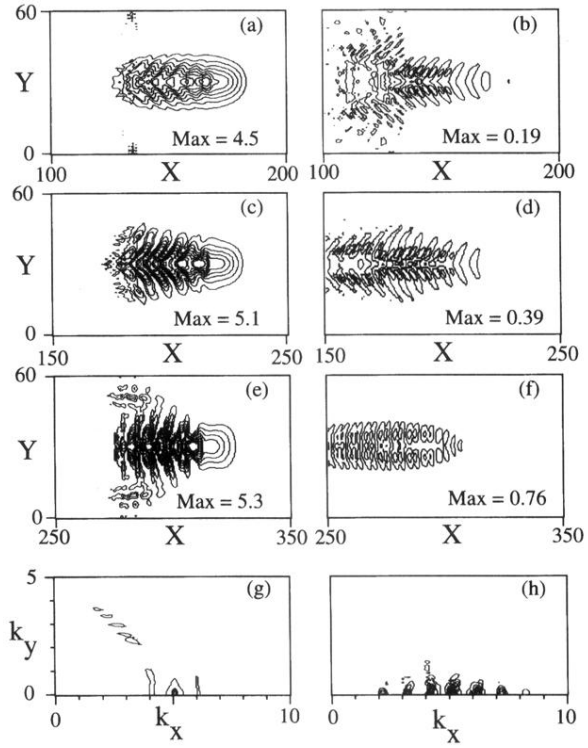

FIG. 3. Contour plots from a 2D simulation with $a_0=0.75$, $\omega/\omega_p=5.0$, and $l_0=50c/\omega_p$. (a) laser field $eE_x/mc\omega_p$ and (b) plasma wave field $eE_x/mc\omega_p$ at $\omega_p t=100$; (c) laser field and (d) plasma wave field at $\omega_p t=150$; (e) laser field and (f) plasma wave field at $\omega_p t=250$. The x and y axes are in units of c/ω_p. Fourier spectrum of laser field at (g) $\omega_p t=250$ and (h) $\omega_p t=250$. Both k_x and k_y in units of $k_p=\omega_p/c$.